Prototype Raman Spectroscopic Sensor for *in Situ* Mineral Characterization on Planetary Surfaces

ALIAN WANG,* LARRY A. HASKIN, and ENRIQUETA CORTEZ

Department of Earth and Planetary Sciences and McDonnell Center for the Space Sciences, Washington University, St. Louis, Missouri 63130 (A.W., L.A.H.); and Analytical Sciences Center, Monsanto Company, St. Louis, Missouri 63167 (E.C.)

Raman spectroscopy has the potential to provide definitive identification and detailed characterization of the minerals that comprise rocks and soils on planetary surfaces. We have designed a probe head for Raman spectroscopy that is suitable for use on a spectrometer deployed by a rover or a lander on the surface of a planet such as Mars, the Moon, or an asteroid. The probe head is lightweight, low power, rugged, and simple. It is based on a tiny distributed feedback diode laser and volume holographic components. A protective shell surrounds the probe head and serves as a mechanical stop for the mechanical arm of a planetary rover or lander during placement of the probe head onto the surface of a rock or soil. Pressing the shell against the rough surface of a target rock or soil also places the sampling objective of the probe head in rough focus, and the probe head is designed to be tolerant of focusing errors of ~5 mm. A breadboard version of the probe head gave spectra of high quality on clean crystals of diamond, sulfur, calcite, quartz, and olivine. The results are qualitatively comparable to those obtained by using a conventional micro-Raman spectrometer on fine-grained travertine and on difficult specimens of basaltic lavas and impactites whose original mineralogy had been altered by reaction with water and air.

Index Headings: **Raman spectroscopy; Raman sensor for planetary mineralogy; *In situ* rock characterization by Raman spectroscopy.**

INTRODUCTION

Seventy years after C. V. Raman[1] discovered the scattering effect that bears his name, Raman spectroscopy is on the verge of becoming a field tool for the geologist. During the pre-laser period, the intrinsic weakness of Raman signals and the state of the art of instrumentation limited Raman spectroscopic studies to samples that were optically homogeneous over a relatively large volume (e.g., gases, liquids, and high-quality crystals). Few geological samples have these optical qualities. The development of laser-based micro-Raman techniques in 1975[2,3] led to an increase in the sensitivity of dispersive Raman spectroscopy of ~10^4 times, which allows heterogeneous and complex geological samples to be examined. The number of publications in geological fields since 1975 is almost eight times the total from the previous fifty years.[4] Up to now, for geoscientific applications, Raman spectroscopy has been almost exclusively a laboratory technique. Developments in laser sources, detectors, fiber optics, and volume holographic optical elements in the last ten years have made possible a new generation of Raman spectrometers.[5–12] These Raman systems (such as the products of Chromex, Dilor, Instrument S.A., Kaiser Optical System, Inc., Renishaw, and SpectraCode) have high optical throughput and high detection sensitivity, and they are small in volume, flexible, and robust in structure. The miniaturization made possible by these developments now makes it feasible to build small Raman systems suitable for geological field work.[13] We discuss here the potential use of a rover-based Raman system for *in situ* mineral characterization on planetary surfaces.

Micro-Raman spectroscopy is a powerful technique for determining the structural and compositional features of a wide variety of minerals and rocks. More than one thousand micro-Raman studies of materials of geoscientific interest have now been published, and several compilations of Raman spectra of minerals have been established.[14–16] It has been amply demonstrated that Raman spectroscopic features correlate with mineral structures and compositions.[17,18] Raman spectroscopy can be used for identification of most natural minerals because each group of oxyanionic minerals (e.g., carbonates, sulfates, phosphates, and different types of silicates) and most oxide, sulfide, and hydroxide minerals have their own characteristic Raman spectral patterns.[19–21] The intrinsic narrowness of Raman peaks of most minerals nearly eliminates peak overlap in spectra of mixtures of minerals and thus enables straightforward phase identification from *in situ* measurements on rocks and other complex natural and man-made materials.[13] Micro-Raman probes can provide spectra of fluid or solid inclusions within minerals.[22–24] Shifts in Raman peak position offer approximate compositional information such as end-member proportions in solid solutions (e.g., the Fe/Mg ratio in olivine, the Fe/Mg/Ca ratios in pyroxene, and the Ca/Mg ratio in carbonate),[25–28] and some changes in relative peak intensity indicate the extent of long-range ordering or its disruption in mineral crystals (e.g., vitrification, structural distortion, etc.).[29–31] Raman spectroscopy is now frequently used to monitor phase transitions in ultra-high-tem-

Received 12 September 1997; accepted 20 November 1997.
* Author to whom correspondence should be sent.

0003-7028/98/5204-0477$2.00/0

perature and -pressure experiments (e.g., in diamond anvil cells)[32,33] and in dynamic chemical reactions.[34]

In the planetary arena, Raman spectroscopy was first used as an adjunct to mid-IR spectroscopy to characterize mineralogically lunar samples returned by Apollo missions.[35–38] These studies on individual mineral grains and glassy particles of lunar soils showed that common minerals could be easily identified. On the basis of more recent work, we proposed that Raman spectroscopy be used for on-surface mineral identification on missions to planets, asteroids, and comets, and especially on missions to the Moon and Mars.[13,39] Raman spectroscopy offers unambiguous identification of most major rock-forming minerals, most minor and trace minerals in common rocks, and a broad range of specialized minerals found in ore bodies. It is nearly as definitive as X-ray diffraction spectroscopy, but is much more rapid and requires no sample preparation. Raman spectroscopy can identify organic components and their degradation products all the way to disordered graphite, and this capability is important for seeking residues of possible exobiological activity.[40] As proposed for planetary applications, visible near-IR and Fe-Mössbauer spectroscopy are limited to Fe-bearing minerals,[41] whereas Raman spectroscopy is not. Raman spectra of minerals have far narrower peak widths (~ 20 cm^{-1}, $<5\%$ of the common spectral range of the fundamental vibration modes of minerals) than Vis-NIR and mid-IR spectroscopy[8] ($\sim 20\%$ and $\sim 30\%$), nearly eliminating peak overlaps in polymineralic spectra. Mössbauer spectroscopy[42] detects minerals such as ilmenite ($FeTiO_3$), for which Raman spectroscopy shows poor sensitivity, and metal phases containing Fe, which Raman spectroscopy does not detect. A Raman spectrometer can operate entirely in the visible spectral region, thus simplifying the requirements for instrumentation as compared to those for work in the mid-IR spectral range.

Raman spectroscopy is a good team technique. The information it would provide on a planetary mission would be enhanced by other spectroscopic and chemical data, and vice versa. Planetary Raman spectroscopy as we propose it here is a close-up, microanalytical technique; spot sizes would be <50 μm. In order to obtain information on the heterogeneity of a rock, the most effective means turns out to be a set of multipoint analyses along a traverse.[43] In addition, Raman imaging over a larger area is a promising technique for the future.[44]

Close-up Raman spectroscopy complements spectral methods such as Vis-NIR or mid-IR, for which the instrument can be perched on a rover mast, where it can scan the field of view and provide data that enable selection of rocks deserving of more detailed analysis. The synergy with Mössbauer spectroscopy has already been mentioned. The combination of Raman spectroscopy and Mössbauer spectroscopy provides essentially complete mineral identification and quantification in rocks and soils, more than either can achieve as a stand-alone instrument.

To demonstrate the feasibility of Raman spectroscopy as a capable method for on-surface planetary mineralogy, we have been working along two lines. One is to simulate planetary experiments using a laboratory spectrometer and appropriate geological samples such as lunar rocks and soils, martian meteorites, and terrestrial samples considered to be good martian analogs. We have successfully demonstrated that four types of first-order information can be obtained by Raman spectroscopic analyses. These are mineral (phase) identification,[13,39] cation ratios of some solid-solution minerals (e.g., Fe^{2+}/Mg^{2+} in olivines and $Fe^{2+}/Mg^{2+}/Ca^{2+}$ in pyroxenes),[13,28] mineral proportions in mixtures[43] (most rocks and soils are mechanical mixtures of mineral phases; few are monomineralic), and rock texture (the spatial relationships among mineral grains).[43] We have made a preliminary study of a terrestrial basalt coated with "varnish".[45] Rock varnish is a surface material whose chemical composition is usually unrelated to the underlying mineralogy but does reflect past or present climatic and surface conditions. The second approach to evaluating Raman spectroscopy as a tool for on-surface planetary mineralogy is to design a Raman spectrometer suitable for on-surface use.[46] This paper describes studies undertaken to date with emphasis on instrumental design.

A RAMAN PROBE HEAD FOR PLANETARY ON-SURFACE MINERALOGY

We have built and tested a breadboard probe head of the type we believe is optimal for planetary on-surface mineralogy. The design, the choice of components, and the characteristics of this device are described below. The probe head can be packaged in a cylinder that is roughly $9 \times 5 \times 5$ cm, small enough for deployment by the mechanical arm of a planetary lander or rover. It would also be useful for terrestrial field studies.

Basic Design Considerations. Among the criteria that an on-surface planetary analytical instrument must fulfill are small volume, low mass, and low power consumption. The instrument must also be stable against the mechanical stresses of travel, which include large excursions in temperature and pressure, strong vibrations during launch and acceleration, jarring during separation of rocket stages and on deceleration and landing, and irregular jolts and vibrations during rover travel. The system must function properly under the harsh environmental conditions of temperature cycling, vacuum or low or high atmospheric pressure, irradiation by cosmic rays, and possible bombardment by micrometeorites. The design of the system should be mechanically simple, with no or few moving parts. Specific criteria for an on-surface Raman system capable of definitive mineral characterization include low background and high sensitivity for Raman shifts in the 200–1700 cm^{-1} spectral region (for oxyanions and carbonaceous materials) and in the 2500–4000 cm^{-1} region (for hydrogen bonded to O, C, N, S, etc.), a wavenumber precision better than 2 cm^{-1}, a spectral resolution of about 4 cm^{-1}, and an internal standard for wavenumber calibration. The mechanical arm of the planetary lander or rover must position the spectrometer properly on the target rock or soil, and this procedure may require some flexibility of the spectrometer on its mounting.

A convenient configuration for an on-surface Raman system is one that divides the instrument into two parts—a lightweight, easily deployable probe head attached to the arm of the rover or lander and an energy analyzer mounted on the rover or lander body along with the elec-

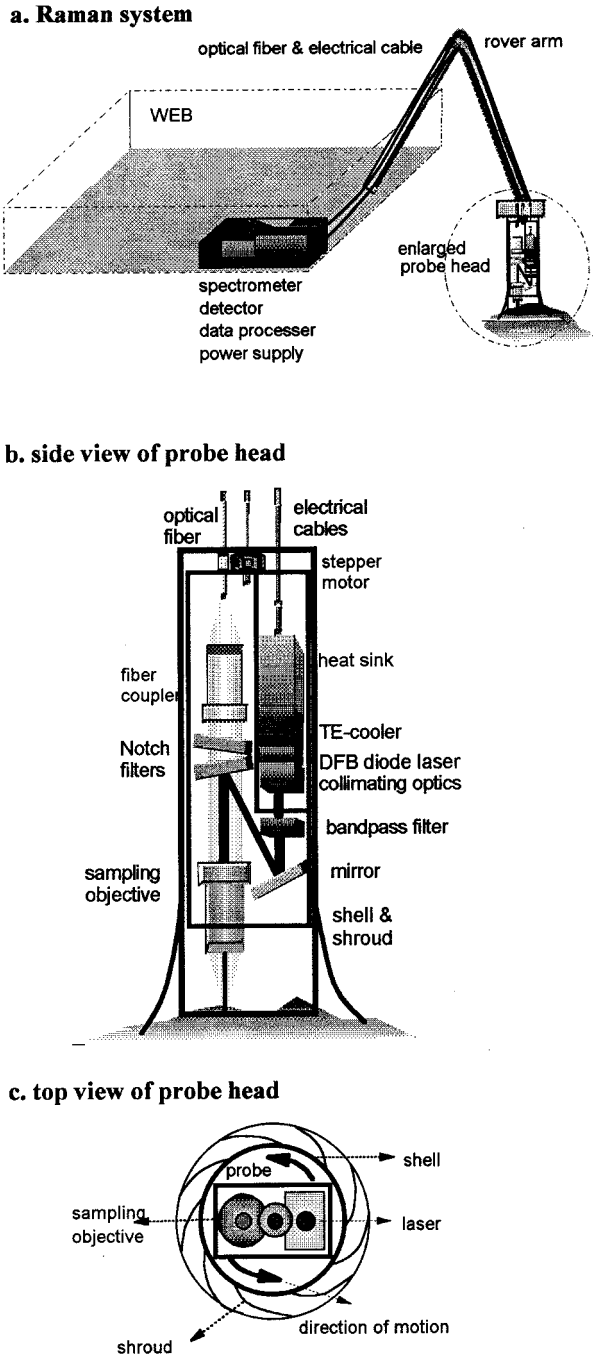

FIG. 1. Schematic diagrams of a robotic Raman system for a planetary rover or lander. (**a**) Probe head at the end of a mechanical arm, deployed against a rock surface, and connected to a spectrograph and power source mounted in a thermally controlled box on the rover or lander. (**b**) Close-up view of probe head showing locations of components. (**c**) Top view of probe head inside its protective shell and showing the flexible shroud at the bottom that serves to decrease ambient light to the collecting objective. Arrows show the rotational motion of the probe head within the shell for point counting.

trical power supply and the data processor (Fig. 1). The two parts are connected by an electrical cable for power and an optical fiber for signal transfer. In this configuration, the probe head produces a monochromatic excitation laser beam (frequency ν_0) and focuses it on the sample. The focusing objective also collects the backscattered radiation from the sample. The probe head then filters out the reflected and Rayleigh scattered ν_0 radiation from the sample and directs the Raman signal through the optical fiber to the energy analyzer. The energy analyzer is a miniaturized spectrograph with a charge-coupled device (CCD) detector. Apart from its miniaturization, it would be similar to commercial models (e.g., HoloSpec *f*/2.2, of Kaiser Optical System, Inc.). In this paper, we report the design and preliminary testing of a breadboard model of the probe head of this Raman system. The mass of this probe head should not exceed a few hundred grams.

Figures 1b and 1c show the basic design of the probe head, which is determined by four main considerations. First, a lensed probe design rather than a fiber-only probe was chosen because of the limited amount of laser power that will be available for a rover- or lander-based Raman system. A microscope objective is used to condense the laser beam to obtain a higher power density at the sampling spot and thus a higher signal-to-noise (S/N) ratio in the spectra and to collect the scattered Raman radiation from the sample. This coaxial light path of excitation and collection ensures maximum cone overlap and thus maximum collecting efficiency of Raman scattered light.

The exciting source, a tiny diode laser, is placed inside the probe head. The fundamental vibrational modes of most minerals, as Raman shifts, lie within the 100–1700 cm^{-1} spectral region, and the main peaks of most oxides and sulfides lie below 600 cm^{-1}. Consequently, a low background level near the backscattered Rayleigh line is important for mineral identification. With the placement of the laser source inside the probe head, the interference in this spectral region from the broad silica Raman band produced within the optical fiber can be avoided. The loss of laser power from the coupling to the fiber can also be avoided by using this approach. In addition, the linear polarization of the laser beam would be retained in this configuration, in contrast to supplying it to the probe head through a high-transmission optical fiber, which would lead to loss of linear polarization. The efficiency of scattering of a polarized laser beam depends (among other things) on the orientation of the mineral crystal. By examining the variation of relative peak heights of a particular mineral, separate but adjacent grains of the same mineral can be identified, which is important to determining the grain size and texture of a rock.[43]

The manner of deployment of a Raman system used on a planetary surface affects the design. Raman spectral measurements will be done on the rough surfaces of rocks and soils as encountered (i.e., without any sample preparation). We assume that the mechanical arm of the rover will only position the Raman probe head by pressing it against the target. For simplicity and ruggedness, no automatic focusing system is provided, but instead the system would use an effective depth of sampling field of several millimeters to accommodate the surface roughness anticipated for most samples. This would be achieved by using a long-working-distance (~ 1 cm), low-numerical-aperture sampling objective, located inside a protective shell around the probe head. This shell would be placed against the target sample by the mechanical arm of the rover or lander and would serve to stop the motion of the arm on contact. The shell would also position the objective in approximate focus with the rock

surface. To compensate for the minor errors of focus resulting from the surface roughness, the arrangement uses an oversized iris at the back-imaging plane (this would be an optical fiber of coarse core). The shell also helps protect the probe head from unintentional contact with surface materials. The edge of the shell would be wedded to a shroud of deformable plastic that would fit the contours of the sample and reduce stray light, enabling daytime operation even under conditions of mediocre signal-to-noise ratios. The shell would also house any components necessary to provide thermal control as required for proper operation of the laser and the volume holographic components of the probe head.

Finally, we have determined that the best way to obtain the proportions of minerals in a rock on a planetary surface is by point counting,[43] a petrographic procedure in which a grid is placed over a thin section of a rock and the identity of the mineral lying beneath each grid point is recorded. The volume proportion of each mineral equals the fraction of the grid points at which that mineral is encountered. To accommodate point counting for detailed mineralogical determinations, a stepper motor at the top of the shell would rotate the probe head inside. This would move the sampling objective, which is offset from the axis of rotation, stepwise along a curved path. A spectrum would be taken at each step along a curvilinear line ~1 cm long in a few hours' time. A small beam size (~20 μm) would be used, so each spectrum would be of one or at most a few mineral grains. This procedure detects minor and trace minerals, as well as minerals whose intrinsic Raman sensitivity is low enough for their signals to be missed if more strongly scattering minerals are simultaneously illuminated by the laser beam. This method also circumvents the problem of scattering geometry, which makes it nearly impossible to convert peak heights in a broad-beam spectrum taken of many grains quantitatively into mineral proportions. This problem arises because signal strength is affected by a wide variety of parameters, such as different Raman cross sections for each constituent mineral, crystal orientation, chemical and structural ordering in the crystal, effective sampling volume (which depends on the position of the laser focus and on the physical properties of the target sample), and general target properties such as surface roughness, grain size, mineral transparency, number of mineral grain boundaries encountered within the sampled volume, and compositional heterogeneity within grains. By producing a linear image of the rock's mineralogy, point counting provides information about rock texture and grain size, both of which are important clues to a rock's origin and history. Two-dimensional Raman imaging of an area of 1 square cm or greater is a promising technique for the future.[44]

The Laser Source. A diode laser would be used as the excitation laser source rather than solid-state or gaseous lasers such as Nd:YAG, Ar^+, and HeNe. A diode laser can be compact in size (a few mm^3), simple in structure, mechanically robust, and efficient in power conversion. Its low operating voltage (2–3 V) is the best choice for battery operation, consonant with use on a rover mission, where power ultimately depends on solar cells. The frequency of laser excitation chosen for this system is a trade-off among several factors. The gallium arsenide diode laser and its derivatives have higher power conversion efficiency [$e_{power}(\nu)$] in the infrared spectral region than in the visible region. The visible region is preferable, however, in terms of Raman scattering efficiency ($e_{Raman} \propto \nu^4$), CCD detection sensitivity of both Raman shift spectral regions to be sensed (100–1700 and 2500–4000 cm^{-1}, Fig. 2a), and reduction of transmission losses through our mainly transmissive optical train. In addition, a visible laser spot on the sample surface, if observed by an imaging system, could determine the location of the Raman measurements relative to those of other instruments covering the same region of the sample. Among the diode lasers of the GaAlAs series that provide visible laser lines, one emitting at 685 nm is selected because it has higher power output than lasers providing shorter wavelengths. A red exciting line also produces lower photoluminescence from rocks than a green line.

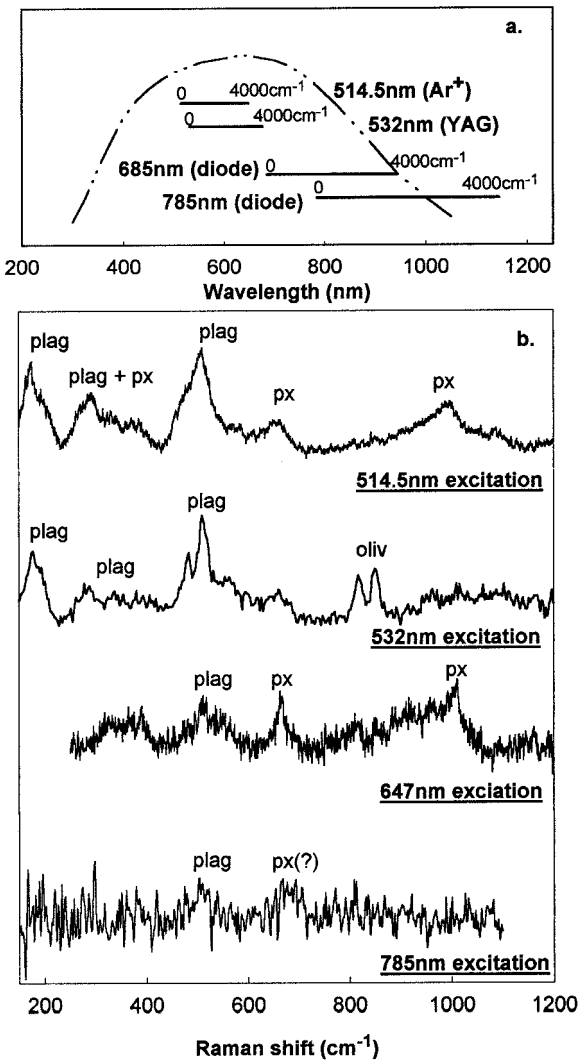

FIG. 2. (**a**) The wavelength ranges over which Raman shifts from rocks would be observed by using different excitation laser lines are compared with the wavelength dependence of sensitivity for a typical CCD (dashed line). (**b**) Spectra from a powdered basaltic lava taken at four excitation wavelengths on different Raman spectrometers.

Figure 2b shows a set of four spectra from a single sample, obtained by four different Raman spectrometers, each using a different excitation laser line (514.5 nm line of an Ar^+ laser, 532 nm line of a diode pumped Nd:YAG

laser, 647 nm line of a Kr^+ laser, and 785 nm line of a diode laser). The sample was a very fine powder (and thus a very poor Raman scatterer) of the common type of lava known as basalt, a plagioclase feldspar-pyroxene rock, and a type of rock common on Mars. Because the spectra were measured with different spectrometers, they are not directly comparable, as they were affected by instrumental factors as well as the exciting wavelengths. It is nevertheless apparent that, with decreasing wavelength of excitation, the S/N of the Raman signal decreases rapidly, mainly because of the ν^4 dependence of the Raman scattering cross section. Also, the photoluminescent background decreases with decreasing excitation wavelength. The 785 nm excitation, under the conditions used, gave a Raman signal that was too weak for definitive mineral identification. Informative spectra were obtained by using the 647 nm excitation line, and with reduced levels of fluorescence as compared with the spectra obtained by using the 514.5 and 532 nm exciting lines.

Ordinary diode lasers exhibit severe frequency shifts (mode hops) if operating temperature or driving current changes. In some commercial Raman systems, an external cavity is combined with the diode laser to produce a stable excitation frequency. However, an additional external cavity increases the size of the laser source substantially and could be sensitive to mechanical vibrations. In practice, for planetary work, this temperature and vibrational sensitivity would be reduced substantially by using a DFB (distributed-feedback) or DBR (distributed-Bragg-reflector) diode laser, for which the longitudinal mode selectivity results from the satisfaction of the Bragg condition of a grating that is etched inside of the diode device itself. Two new types of DFB[47] and DBR[48] lasers have been recently developed that operate in the red spectral region. A laser under commercial development with this configuration (Spectra Diodes, Inc.) has a robust physical structure and a very small size ($8 \times 8 \times 2$ mm) that could easily be accommodated in our probe head. Using a DFB diode laser would also greatly reduce the task of filtering to obtain a purified excitation line. Despite this improved stability, the spectrometer would still require an internal frequency standard, as discussed later.

The linewidth of the central mode of a diode laser is normally <0.003 cm^{-1}, more than adequate for obtaining CCD pixel-limited spectral resolution. On the basis of our simulation experiments,[13,39,43] a spectral resolution of ~ 4 cm^{-1} is sufficient to distinguish among mineral phases and determine peak shifts well enough to provide useful values of cation ratios in mineral solid solutions.

From experiments done with ~ 7 mW of excitation laser power delivered onto a 30–50 μm diameter sampling area, but using a conventional Raman spectrometer equipped with a diode array detector, we can obtain Raman spectra of acceptable quality even from mediocre Raman scatterers with recording times of only a few minutes.[13,39,43] Allowing for a 40% loss of power in collimating, filtering, and transmitting the beam to the sample, we estimate that a 20 mW power output from a diode laser would be enough to yield good spectra from rocks and soils in a time period of minutes. For a diode laser working at 685 nm, 20 mW output power requires a power supply that generates about 400 mW, which is acceptable for an analytical instrument on a planetary rover.

The Optical Train. The beam from a diode laser has a pseudo-Gaussian transverse intensity profile essentially analogous to the TEM_{00} mode of many gas lasers. The small and asymmetric lateral dimensions of the active region (about $3 \times 0.6 \times 300$ μm) of the diode laser result in wide (20° to 40° half angle) and asymmetric (2.5 to 6 times difference between orthogonal directions) divergence angles of the laser beam and thus an elliptical beam cross section. The beam is thus asymmetric and, in many instances, astigmatic. In order to obtain diffraction-limited performance in the optical path, optical corrections to the beam cross section are needed. Collimating optics are required to minimize the divergence angles for propagation of the beam along the optical path, even though that path is very compact in our system. Astigmatism, which has a serious impact on the collimating and focusing performance of a laser beam, is caused by the longitudinal separation between the emission points parallel and perpendicular to the junction of the diode laser, the separation arising from the directional dependence on the refractive index of the lasing cavity. Index-guided lasers that use refractive index boundaries in both directions to define the active region leave almost no astigmatism for near-infrared lasers, and only mild astigmatism for red lasers. This astigmatism can be reduced if necessary through the use of a weak cylindrical lens.

Although the side-mode suppression of a DFB or a DBR laser could reduce side-band signals to as little as 30 dB, a contribution to the background by the spontaneous emission of the diode material could still interfere with the Raman signal from the sample. A bandpass filter effectively removes this background and the side-mode radiation. A dielectric interference bandpass filter is used in this design mainly because it occupies little space. A high-quality filter of this type can provide a factor of $\sim 10^4$ to 10^5 blockage at the two wings and have a transmittance of $\sim 80\%$ at the main laser frequency, a narrow bandwidth, and a very small temperature coefficient of band shift.

The rest of the optical train in our probe head is similar to those in commercially available Raman probe heads. Two Super-Notch-Plus filters (HSPF-685-1.0 of Kaiser Optical System, Inc.) reduce the 685 nm (ν_0) component from the total light collected by the sampling objective by a factor of $\leq 10^{-12}$, with $\sim 80\%$ transmittance for the Raman signal and a bandwidth [full width at half-height (FWHH)] of ~ 220 cm^{-1}. The first Notch filter also serves as a mirror to direct the laser beam into the sampling objective. Several long-working-distance (~ 5 to 10 mm), low-magnification (8× to 50×), and low-numerical-aperture (0.25 to 0.55) microscope objectives were tested as sampling objectives (discussed later). A 10× microscope objective [0.25 numerical aperture (NA)] was used as a coupler to condense the Raman radiation onto a hydroxyl-free, multimode single optical fiber cable (200 μm core diameter, 0.22 NA), which transmits the signal to the spectrograph. In this configuration, the entrance pupil of the optical fiber serves as a spatial filter at the image plane. In a Raman signal-collecting system, the transmission (Θ_T) of the Raman radiation that comes from a sampled location Δ above or beneath the focal plane of the sampling objective can be estimated by using Eq. 1, developed by Dhamelincourt and Barbillat.[49]

$$\Theta_T \approx d/[\Gamma_0(\mathrm{NA} * \Delta + (R_0 * (1 + (\sin^{-1}(\mathrm{NA}) * \Delta)^2)^{1/2}))]^2. \quad (1)$$

In Eq. 1, d is the diameter of the entrance pupil of the spatial filter, NA is the numerical aperture of the sampling objective, R_0 is the size of laser beam spot at the focusing plane, and all distances are in millimeters. Thus, d and NA are the main instrumental factors that determine the effective depth of the sampling field of this system. In order to have a large sampling depth (to tolerate the focusing errors resulting from surface relief of the rocks during *in situ* measurements), a coarse-core optical fiber and a sampling objective with low numerical aperture are preferred. However, a fiber that is too coarse would have low mechanical flexibility and could lead to high light leakage; 200 μm is a good compromise. In addition, an objective with a low numerical aperture leads to a low laser power density at the sample surface and seriously reduces the collecting efficiency of Raman radiation scattered from the sample. Other factors such as the characteristics of the target samples and the match between the sampling and the coupling objectives also influence the strength of the Raman signal and the effective sampling depth in a measurement. Experimental tests to determine optimal combinations of components were done and are described below.

TEST MEASUREMENTS ON MINERALS AND ROCKS

Experimental Setup. A breadboard model of the probe head was constructed in our laboratory to demonstrate proof of concept; no effort was made to package the components into the small volume required for planetary on-surface use. An ordinary GaAlAs diode laser (Melles Griot 56DOL663, ~683 nm, 28 mW output) served as the excitation source because no red DBR or DFB laser was yet available. By controlling the operating temperature and driving current closely, we obtained an excitation output from this diode with a frequency stability of 683 ± 0.07 nm in the laboratory. An isolator was added into the breadboard model, to prevent any change that might have occurred in the condition of lasing resulting from light feedback from a highly reflective sample. This precaution would not be necessary if a DFB or DBR laser were used.

In order to test the performance of this breadboard model of the probe head, the Raman signal collected by it was sent into the third stage of a 1877 Triplemate (Spex company) spectrograph, which has an asymmetric Czerny–Turner configuration, 0.6 m focal length, *f*/6.3 aperture, and 870 cm^{-1} spectral coverage obtained by using an 1800 groove/mm grating, and is equipped with a back-thinned L-N_2 cooled CCD detector (2000 × 800 pixel). The Raman output from the optical fiber (0.22 NA) of the probe head was coupled into the entrance slit (d = 300 μm) of the spectrograph by using a simple 1 in. diameter, 1 in. focal length bi-convex lens. A considerable fraction of the collected Raman signal was lost in this coupling, because of the large difference between the f number of the spectrograph and that of optical fiber, along with the very tight space available in the spectrometer, which did not enable the position of the coupling bi-convex lens to be optimized. (The breadboard model was designed to connect to a spectrograph with greater light-gathering capacity such as *f*/2.2; thus, we have not tested the probe head under conditions of high detection sensitivity.) An 8× Nachet objective (NA = 0.25) was used as sampling objective for most of these tests. Because the ~15 mW, ~683 nm laser beam has an elliptical cross section (about 7.85 × 1.57 mm at $1/e^2$ intensity), it did not cover the entire entrance pupil of that sampling objective, so the size of the condensed laser spot on the sample surface was about 25 × 5 μm, as estimated by using the *effective* numerical aperture for an under-filled objective (P. Dhamelincourt, private communication). The sample was placed on an XYZ-adjustable microstage and was brought as near as possible to the focal plane of the objective visually but without the use of a microscope image. Laser focusing errors thus ranged as high as a few millimeters, which is the same magnitude as the focusing ability of the rover arm with the use of the mechanical stop (the shell of probe head). Despite the less than optimal conditions of the tests, good mineral spectra were obtained within reasonable dwell times on the sample, as described below.

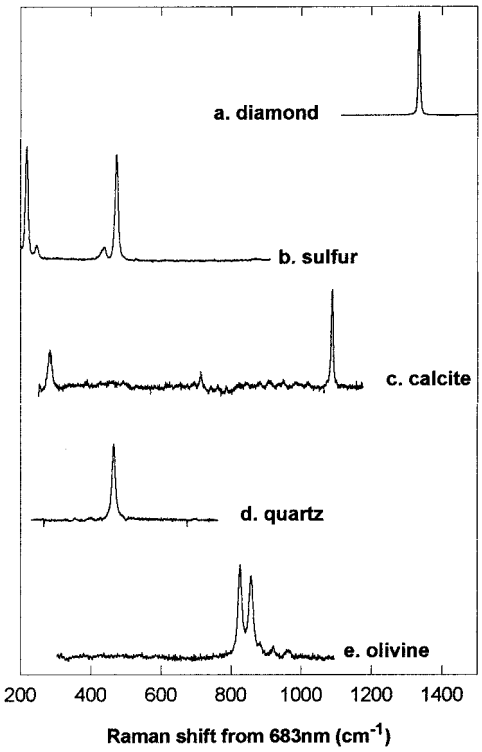

FIG. 3. Raman spectra of minerals obtained using the breadboard model of the prototype planetary probe head: (***a***) diamond; (***b***) sulfur; (***c***) calcite; (***d***) olivine; (***e***) quartz.

Measurements on Minerals. Spectra of five minerals—diamond, sulfur, calcite, quartz, and olivine—were taken in this instrument configuration (Fig. 3). These minerals were selected on the basis of their excellent properties as Raman scatterers (diamond and sulfur) or their common occurrence in geological settings (calcite, quartz, and olivine). Diamond and sulfur are particularly strong Raman scatterers, and their peaks provided the best guide to improving the optical alignment of our breadboard system.

Diamond has a single, strong, narrow Raman peak at

1332 cm^{-1} with an FWHH of 6 cm^{-1} in our experimental setting. A small diamond chip was used as an internal frequency standard. The height of the diamond peak was also used to monitor intensity, to ensure that the alignment of the optics remained optimized. We would place a diamond chip in the optical train of our planetary probe head for the same purpose. Diamond is mechanically rugged and chemically stable under martian surface conditions. No oxidation of a small grain was observed under a laboratory air atmosphere even when a very high laser power density of ~15 000 W/mm^2 was used. The temperature coefficient of diamond is low, so the peak wavelength will shift by a negligible amount over the temperature range that would be encountered on Mars.

Sulfur has several strong Raman peaks and, in conjunction with diamond, provided a range of wavelengths from 218 to 1332 cm^{-1} for system testing. In our experimental setup, the lowest wavenumber sulfur peaks could not be observed, mainly because of the relatively inefficient suppression of side-mode radiation in the beam of the ordinary diode laser and the wide bandwidth (±5 nm, FWHH) of the bandpass filter used in this breadboard model, which allowed some of these unwanted wavelengths to pass with only weak attenuation (the ±173 cm^{-1} region about the 683.2 nm laser line has a transmittance of >1%). These emissions had to be removed downstream by the two Notch filters (bandwidth ~222 cm^{-1}) used to remove the backscattered and reflected light of the exciting wavelength. Small, sharp peaks from the side modes were seen in rock spectra with particularly low S/N, but did not appear in spectra with high S/N (e.g., Fig. 3). Using a DFB laser as the excitation source will eliminate this problem.

A bandpass filter with a narrower bandwidth (about ±2 nm) would allow detection of Raman lines at lower wavenumbers, but at a cost of increased temperature sensitivity and decreased throughput. Given the harsh environment of a planetary surface, the difficulty of tight temperature control for an arm-based probe head, and the relatively low scattering efficiencies of rocks and soils, sacrificing low-wavenumber detection (<200 cm^{-1}) rather than more general detection sensitivity is preferred. For the purpose of identification of major rock-forming minerals and carbonaceous materials, a spectral range beginning at 200 cm^{-1} is sufficient.

Calcite and other carbonates are important minerals to seek on the surface of Mars, because on Earth their formation is associated with water and sedimentary and hydrothermal processes. Calcite is a strong Raman scatterer, with its main peak near 1088 cm^{-1}. With the use of our breadboard model coupled with a conventional spectrograph, the Raman spectrum of calcite was obtained without difficulty. Its three spectral peaks (1088, 714, 282 cm^{-1}, spectrum c, Fig. 3) provide enough information to distinguish trigonal calcite ($CaCO_3$) from other carbonates with different cations [e.g., $CaMg(CO_3)_2$, $MgCO_3$, $CaFe(CO_3)_2$, $FeCO_3$, etc.] and to distinguish calcite from aragonite, the low-temperature, monoclinic form of $CaCO_3$. Aragonite often forms by precipitation in hot springs. A Raman system with a spectral region beginning above ~200 cm^{-1} would miss the 207 cm^{-1} peak of aragonite, but the aragonite double peak near 708 and 704 cm^{-1} would still be diagnostic.

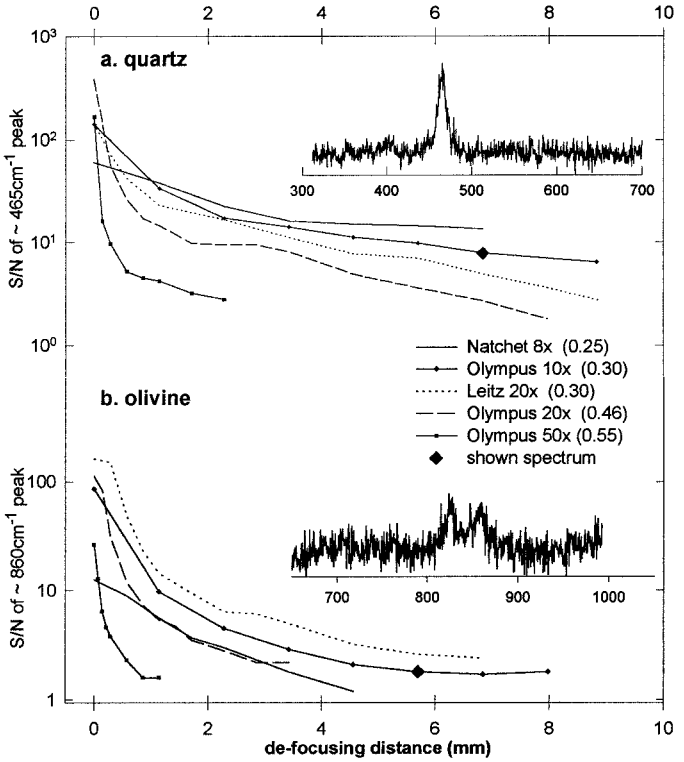

FIG. 4. The effective depth of the sampling field for Raman spectroscopy as obtained by using different sampling objectives with targets of (***a***) quartz; and (***b***) olivine.

Silicate minerals are the principal constituents of the inner circle planets and most asteroids and may be present at almost all surface sites selected for geological study. The ability to obtain information on the chemical and mineral compositions of silicates is therefore a must for an on-surface planetary mineralogical instrument. Raman spectra of two silicate minerals, olivine [$(Fe,Mg)SiO_4$] and quartz (SiO_2), were obtained with fairly good S/N ratio (spectra d and e in Fig. 3). Tests to determine effective depth of sampling field by measuring peaks from those two silicates are described below.

Effective Depth of Sampling Field Using Different Objectives. As discussed above, a large depth of sampling field (i.e., tolerance of focusing errors) is important for an uncomplicated probe head designed for use on a rover-based Raman system. To determine the sampling depth of our breadboard model, we did the following experiment. The quartz or olivine grain, mounted on an XYZ-adjustable micro-stage, was brought into the focal plane of the excitation laser beam. A Raman spectrum was recorded; then the micro-stage was moved away from the focal plane in increments of 0.285 mm. This process was repeated until the characteristic Raman peak of the sample became nearly indistinguishable from the spectral background. Signal-to-noise ratios of the ~820 and ~860 cm^{-1} doublet of olivine and the 465 cm^{-1} peak of quartz were used as the criteria for determining the range of the effective depth of sampling field. Five series of measurements were done by using objectives with different magnifications and numerical apertures but keeping all other optical elements the same (i.e., the 1 in. diameter Notch filters, the 10× coupling objective with

NA of 0.25, and the 200 μm diameter single optical fiber). The olivine and quartz specimens used in these tests have large enough grain sizes and overall sample thicknesses (~ 2–3 mm) to ensure that the effective depth of sampling field is determined mostly by instrument characteristics rather than sample characteristics.

Figure 4a shows the S/N ratio of the main quartz peak as a function of defocusing distance in millimeters for five microscopic objectives: 8× Nachet, 0.25 NA; 10× Olympus, 0.3 NA; 20× Olympus, 0.3 NA; 20× Leitz, 0.46 NA; and 50× Olympus, 0.55 NA. Figure 4b shows analogous curves for olivine as the test sample. These curves show that the S/N ratio of Raman peaks decreases as expected as the distance away from optical focus increases. Similar results were obtained when the sample was too near the objective for proper focus. The behaviors are similar for those objectives that have similar numerical apertures; thus, the 20× Leitz objective with an 0.30 NA is more similar to the 10× Olympus objective with a 0.3 NA than to the 20× Olympus objective with a 0.45 NA. With high magnification and numerical aperture of the sampling objective (20× Olympus and 50× Olympus), the S/N ratio of spectra recorded at laser focus is high, but it decreases rapidly by the point at which the sample-to-objective distance has been changed by 1–2 mm away from focus; i.e., the effective depths of sampling field are relatively shallow. In the case of the 50× Olympus objective, the diameter of the output beam so greatly exceeded the entrance pupil of the 10× (0.25 NA) coupling objective to the fiber that a large fraction of the collected Raman signal was lost. The low-magnification 8× Nachet 0.25 NA objective has very large depth of sampling field (S/N ~ 13.5 at 6.84 mm defocusing distance for quartz), but its detection sensitivity is relatively low.

For the optical characteristics of our breadboard, the 0.3 NA, low-magnification objectives (10× or 20×) offer both high detection sensitivity and excellent tolerance of defocusing and are therefore reasonable choices for the type of robotic applications we envision. The quartz spectrum shown in the upper part of Fig. 4a was recorded by a 10× Olympus objective defocused by 6.84 mm (diamond-shaped point on the curve). An unambiguous identification of quartz could thus be made even with a focusing error of ±7 mm; the same is true at ±6 mm for olivine.

Simulating Measurements on Rocks. Six rock samples were used for simulation measurements. The measurements on calcite, olivine, and quartz were sufficient demonstration that the probe head could readily obtain data of high quality from fresh or well-preserved igneous and sedimentary rocks. Thus, the main testing of the probe head was on rocks intentionally chosen as difficult specimens of types of rocks one might expect to encounter on Mars. This group included the specimen that gave the poorest results of the many we have examined using a conventional micro-Raman spectrometer. All the specimens used in the test were relatively fine-grained, which would give low S/N under the best of conditions, and the original mineralogies of all except the travertine sample and the Ortenberg basalt had been substantially altered by reaction with air and water. Some of the rocks accessible at the martian surface may be analogously altered, and it is important to know how their present mineralogy can be determined. The samples used were unsawn pieces with rough surfaces, from which only strongly weathered surface material had been chipped off (because, on Mars, sand blasting should prevent the buildup of thick rinds). Overall, this was a tough set of tests for the prototype planetary probe head.

The measurements were of two types. In the first type, the intent was to make the best measurements possible on these rocks. Distinguishable parts of the rocks were targeted visually, mainly on the basis of color. The beam focus was adjusted by taking several test spectra; then a final spectrum was recorded at the optimum objective to sample distance. For the other type of measurement, the rock surface was placed in rough focus; then the rock was moved randomly and spectra were recorded without adjustment of the laser focus or selection of favorable sampling locations. This type of measurement is similar to the *in situ* measurement on a planetary surface as it would be done by a robotic Raman system.

Optimized Measurements. One class of rocks expected on Mars is impactite, material produced by explosive shattering of rock by an impacting meteoroid and partly or entirely melted or sufficiently sintered to produce a durable rock. For this test, an impactite from the Manson, Iowa, impact structure was used. The matrix of the rock crystallized from an impact melt, and it has undergone some post-formational hydrothermal alteration. It is fine-grained and consists mainly of quartz and potassic feldspar. Raman peaks from those minerals are readily seen in the recorded spectra [spectra A(1) and A(2), Fig. 5]. A vein crosses the specimen; it was identified from its Raman spectrum as calcite [spectrum A(3), Fig. 5]. Despite the relatively small beam size (25 × 5 μm), mixed spectra of quartz and K-feldspar were recorded at several locations, which suggests an intergrowth relationship between those two minerals. The spectrum obtained at the boundary of the vein contains clear signals from all three minerals.

A second sample tested was a hydrothermally altered Keweenawan basalt, which has a reddish, fine-grained matrix, two coarse amygdules (holes) filled with white minerals, and many small flecks of a light-gray material embedded in the matrix. The spectrum obtained from the matrix [spectrum B(1), Fig. 5] shows a mixture of partly altered pyroxene (still showing the 670 cm^{-1} peak) and an alteration product of pyroxene having two main peaks near 620 and 290 cm^{-1} (an Fe-bearing oxide). The minerals filling the amygdules are calcite [spectrum B(2)] and a zeolite mineral, thomsonite [$NaCa_2(Al_2Si_2O_8)_{2.5}\cdot 2H_2O$, spectrum B(3)]. The light gray flecks inside the matrix [spectrum B(4), Fig. 5] show two main peaks near 680 and 360 cm^{-1}, characteristic of phyllosilicate minerals (probably a clay).

The third rock chip tested was an olivine tholeiite basalt with phenocrysts of olivine and plagioclase from Ortenberg, Germany. The only spectral features observed from most of the points measured were peaks of olivine (spectrum C, Fig. 5). For reasons still unknown, peaks for plagioclase, the other principal mineral of the rock, were not observed. They were also not observed when a conventional micro-Raman spectrometer was used. For reasons not yet known, this rock gives the poorest re-

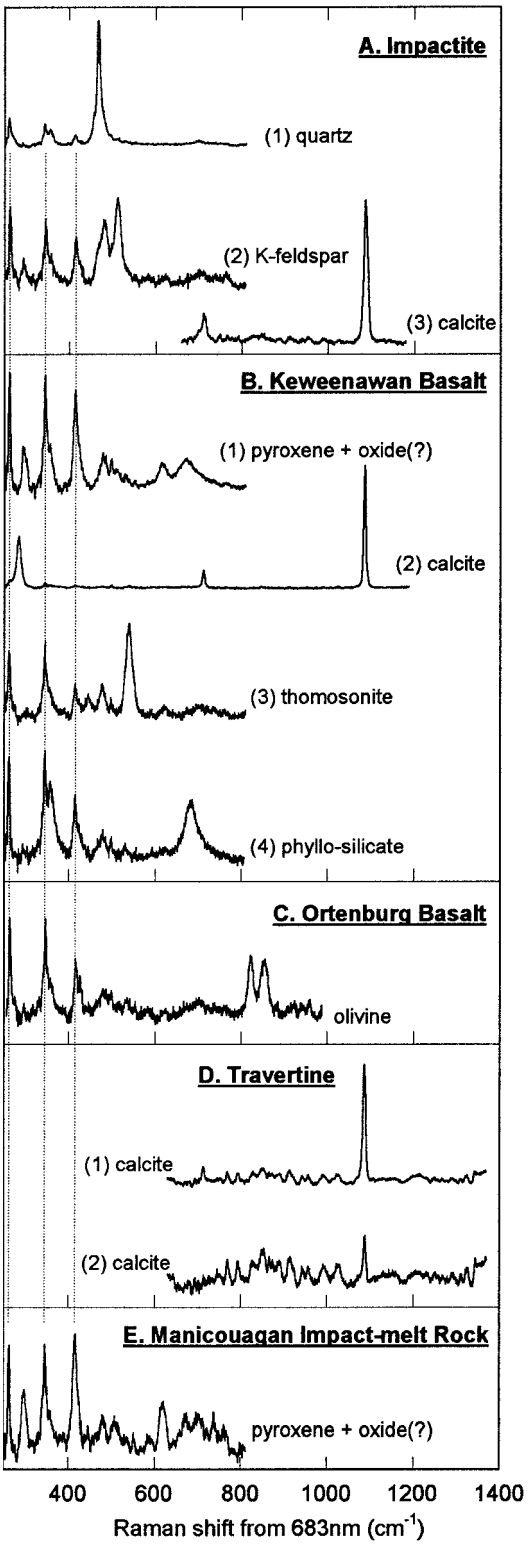

FIG. 5. Raman spectra of altered and fine-grained rocks used as a tough test of the breadboard model of the probe head: (**A**) An impactite from Manson impact structure; (**B**) a hydrothermally altered Keweenawan basalt; (**C**) Ortenberg basalt; (**D**) micro-crystalline calcite-variety travertine; (**E**) a Manicouagan impact melt rock chip. All spectra show the presence of side-mode radiation from the laser (the vertical dashed lines show their positions). In some spectra, apparent peaks corresponding to uncorrected detector response appear (e.g., the travertine spectra).

sponse we have encountered among the many we have examined by Raman spectroscopy so far; even so, it did give a recognizable olivine signal.

Random Point Spectra. Four sets of ~ 10 spectra each were taken at random points and with rough focus on each of four rock chips. One set was from a travertine (micro-crystalline calcite of hydrothermal origin). In addition to its fine-grained texture, the surface of this rock had considerable relief and was tilted at an angle to the beam. The spectra from all 10 measurements nevertheless showed the characteristic Raman spectral pattern of calcite, with changes in the S/N ratio from spot to spot. Spectrum D(1) in Fig. 5 was recorded from a surface tilted at an angle of ~ 15° to the normal to the incident laser beam. The lower spectrum, D(2), was recorded from another location, where the surface tilted at an angle of ~ 70°. Mineral identification was readily achieved from inspection of the raw spectra. Comparing these spectra with the spectrum recorded from a single calcite crystal grain (spectrum c, Fig. 3) shows that the grain size, surface roughness, and surface tilting are all important factors affecting the S/N of a rock spectrum.

Eleven random spots were measured on the same fragment of hydrothermally altered Keweenawan basalt that was used for the optimized measurements. These spots yielded three spectra of calcite and thomsonite (zeolite), two spectra of phyllosilicates, and six spectra of mixed phases showing features of pyroxene and its alteration products (Fe-bearing oxides)—basically, the same results as observed in the optimized test and shown in Fig. 5B. These spot measurements indicate that good point counts could be made to obtain the major mineral components and their proportions in this rock.

Ten spots were measured on an impactite from the Manicouagan impact structure. This impactite formed from an impact melt and is more hydrothermally altered than the impactite from the Manson structure. Although the rock contains plagioclase, K-feldspar (sanidine), pyroxene, quartz, smectite, and hematite, all spots yielded similar spectral patterns (spectrum E, Fig. 5), with two main peaks near 620 and 290 cm^{-1}, Fe^{3+} -bearing alteration products and pyroxene.

Overall, these tests show that, even for the majority of these difficult test samples, the probe head and associated spectrometer provided spectra from which the principal minerals and their alteration products could be identified. Even the especially difficult Ortenberg basalt yielded identifiable olivine spectra. The prototype planetary probe head is obviously not the equivalent in capability to the microscope-based sampling system of a conventional micro-Raman spectrometer. For its intended purpose, identification of minerals in chips of rocks, however, the outcome from the use of the probe head was the same as the outcome obtained with a micro-Raman spectrometer. That the Ortenberg basalt gave poor data was not a failure of the probe head designed for use on planetary surfaces, but a consequence of the poor Raman scattering characteristics of the rock. Raman studies of meteorites from Mars using a conventional micro-Raman spectrometer (unpublished results) yielded excellent spectra of pyroxene and shocked plagioclase (maskelynite), indicating that at least some common Mars rocks have

far better Raman scattering characteristics than the worst of the analogs tested in this work.

CONCLUSION

The spectra described above demonstrate that the excitation and collection system designed to meet the requirements for on-surface planetary mineral characterization (small size, low power consumption, limited focusing ability) works well. Because of the nature of the rock specimens used, this was a tough test, not only for the probe head, but of Raman spectroscopy as an on-surface instrument for planetary mineralogy, as well. The rocks examined were not fresh igneous rocks or well-preserved sedimentary carbonates, but fine-grained travertine and fine-grained lavas and impactites with altered mineralogies. All rocks measured gave useful Raman spectra, and the ability to make those measurements supports the case for robotic mineral determination by Raman spectroscopy. Much better Raman spectra are obtained on fresh surfaces of unaltered rocks—for example, on a chip of lunar basaltic rock.[28] The extent of alteration of rocks on Mars is unknown, except that hydrated Fe^{3+} compounds appear to dominate the spectral features of large areas of the planet, probably in the form of a surface veneer of oxidized material spread by martian dust storms.

ACKNOWLEDGMENTS

We thank Paul Dhamelincourt, Wm. H. Smith, Hua Li, and Michael Pelletier for instructive comments on optical design. We thank Kevin Davis of Kaiser Optical Systems, Inc. and Howard Schaffer of Instrument S.A. for doing the measurements using 532, 785, and 647 nm excitation laser lines. We thank Jill Pasteris and Brigette Wopenka for the use of their Raman spectrometers. This project was supported in part by the National Aeronautics and Space Administration through Grants NAGW 5207 and NAG 5-4642.

1. C. V. Raman and K. S. Krishnan, Nature **121,** 501 (1928).
2. M. Delhaye and P. Dhamelincourt, J. Raman Spectrosc. **3,** 33 (1975).
3. G. J. Rosasco, E. S. Fitz, and W. A. Cassatt, Appl. Spectrosc. **29,** 396 (1975).
4. GeoRef, (American Geological Institute, Alexandria, Virginia, 1996).
5. I. R. Lewis and P. R. Griffiths, Appl. Spectrosc. **50,** 12A (1996).
6. J. M. Tedesco, H. Owen, D. M. Pallister, and M. D. Morris, Anal. Chem. **65,** 441A (1993).
7. B. Chase, Appl. Spectrosc. **48,** 14A (1994).
8. M. Myrick and S. Angel, Appl. Spectrosc. **44,** 565 (1990).
9. C. Allred and R. McCreery, Appl. Spectrosc. **44,** 1229 (1990).
10. C. Schoen, T. Cooney, S. K. Sharma, and D. Carey, Appl. Opt. **31,** 7707 (1992).
11. S. K. Sharma, C. L. Schoen and T. F. Cooney, Appl. Spectrosc. **47,** 377 (1993).
12. T. F. Cooney, H. T. Skinner, and S. M. Angel, Appl. Spectrosc. **50,** 3513 (1996).
13. A. Wang, B. Jolliff, and L. A. Haskin, J. Geophys. Res.—Planets **100,** 21189 (1995).
14. H. J. Schubnel, M. Pinet, D. C. Smith, and B. Lasier, Zeitschrift der Deutschen Gemmologischen Gesellschaft **41,** 178 (1992).
15. A. Wang, J. Han, L. Guo, J. Yu, and P. Zeng, Appl. Spectrosc. **48,** 959 (1994).
16. C. Beny, A. M. Gallas, B. Lasnier, and R. A. Maestrati, "A Catalogue of Raman Spectra of Natural and Synthetic Minerals and their Varieties: A Useful Tool for the Application of Raman Spectrometry in Fields of Earth Sciences and Industrial Mineralogy", in Abstract of the International Mineralogical Association, 16th general meeting (1994), p. 40.
17. W. P. Griffith, "Raman Spectroscopy of Minerals", in *The Infrared Spectra of Minerals,* V. C. Farmer, Ed. (Mineralogical Society, London, 1974), p. 119.
18. W. P. Griffith, "Advances in the Raman and Infrared Spectroscopy of Minerals", in *Spectroscopy of Inorganic-Based Materials,* Advances in Spectroscopy Vol. 14, R. J. H. Clark and R. E. Hester, Eds. (Wiley and Sons, Chichester/New York, 1987), p. 119.
19. W. P. Griffith, Nature (London) **224,** 264 (1969).
20. W. P. Griffith, J. Chem. Soc., A, Inorg., Phys., Theor. **9,** 1372 (1969).
21. W. P. Griffith, J. Chem. Soc. A, Inorg. Phys., Theor. **10,** 286 (1970).
22. J. D. Pasteris and B. J. Wanamaker, Am. Mineral. **73,** 1074 (1988).
23. J. Dubessy, B. Poty, and C. Ramboz, Eur. J. Mineral. **1,** 517 (1989).
24. M. L. Dele-Dubois, P. Dhamelincourt, J. P. Poirot, and H. J. Schubnel, Revue de Gemmologie A.F.G. **88,** 13 (1986).
25. W. D. Bischoff, S. K. Sharma, and F. T. Mackenzie, Am. Mineral. **70,** (1985).
26. F. Guyot, H. Boyer, M. Madon, B. Velde, and J. P. Poirier, Phys. Chem. Miner. **13,** 91 (1986).
27. A. M. Hofmeister, and A. Chopelas, Phys. Chem. Min. **17,** 503 (1991).
28. A. Wang, B. L. Jolliff, K. M. Viskupic, and L. A. Haskin, "Raman Spectroscopic Characterization of Different Types of Pyroxene", in *Lunar and Planetary Sciences XXVIII,* Paper presented to the Twenty-Eighth Lunar and Planetary Science Conference (Lunar and Planetary Institute, Houston, Texas, 1997), p. 1491.
29. A. Wang, W. Wang, and A. Zhang, Can. Mineral. **29,** 517 (1991).
30. P. F. McMillan, G. H. Wolf, and P. Lambert, Phys. Chem. Min. **19,** 71 (1992).
31. M. Miyamoto and K. Ohsumi, Geophys. Res. Lett. **22,** 437 (1995).
32. H. K. Mao, and P. M. Bell, "Experiment for in Situ High-Pressure, Light-Scattering Measurements", in *Year Book of Carnegie Institution of Washington* (Carnegie Institution of Washington. Washington, D.C. 1980), Vol. 79, p. 411.
33. R. J. Hemley, H. K. Mao, and E. C. T. Chao, Phys. Chem. Min. **13,** 285 (1986).
34. J. D. Frantz, J. Dubessy, and B. O. Mysen, Chem. Geol. **116,** 181 (1994).
35. C. H. Perry, D. K. Agrawal, E. Anastassakis, R. P. Lowndes, and N. E. Tornberg, Geochim. Cosmochim. Acta **3,** 3077 (1972).
36. G. W. Fabel, W. B. White, E. W. White, and R. Roy, Geochim. Cosmochim. Acta **3,** 939 (1972).
37. W. B. White, "Structural Interpretation of Lunar and Terrestrial Minerals by Raman Spectroscopy", in *Infrared and Raman Spectroscopy of Lunar and Terrestrial Minerals,* C. Karr, Jr., Ed. (Academic Press, New York, 1975), p. 325.
38. C. H. Perry and R. P. Lowndes, "Elastic and Inelastic Light Scattering Spectra of Lunar Rocks and Soils", in *Infrared and Raman Spectroscopy of Lunar and Terrestrial Minerals,* C. Karr, Jr., Ed. (Academic Press, New York, 1975), p. 273.
39. B. L. Jolliff, A. Wang, and L. A. Haskin, "Identification of Minerals in Several Martian Surface Analog Materials by Raman Spectroscopy", in *Lunar and Planetary Sciences XXVIII,* Paper presented to the Twenty-Eighth Lunar and Planetary Science Conference (Lunar and Planetary Institute, Houston, Texas 1997), p. 675.
40. T. J. Wdowiak, D. G. Agresti, S. B. Mirov, A. B. Kudryavtsev, L. W. Beegle, D. J. Des Marais, and A. F. Tharpe, Abstract for Conference on Early Mars: Geologic and Hydrologic Evolution, Physical and Chemical Environments, and the Implications for Life, LPI Contribution Number 916, Houston, Texas (1997), p. 81.
41. R. G. Burns, *Mineralogical Applications of Crystal Field Theory* (Cambridge University Press, Cambridge, 1993), 2nd ed., Chap. 10, p. 396.
42. S. S. Hafner, "Mössbauer Spectroscopy in Lunar Geology and Mineralogy", in *Topics in Applied Physics,* Vol. 5, *Mössbauer Spectroscopy,* U. Gonser, Ed. (Springer-Verlag, New York, 1975), p. 167.
43. L. A. Haskin, A. Wang, K. M. Rockow, B. L. Jolliff, R. L. Korotev, and K. M. Viskupic, J. Geophys. Res. **102,** 19293 (1997).
44. H. R. Morris, C. C. Hoyt, P. Miller, and P. J. Treado, Appl. Spectrosc. **50,** 805 (1996).
45. E. J. Israel, R. E. Arvidson, A. Wang, J. D. Pasteris, and B. L. Jolliff, J. Geophys. Res.–Planets, paper in press.
46. A. Wang, E. Cortez, and L. A. Haskin, "A Raman Spectroscopic Sensor for On-Surface Planetary Remote Sensing", in *Lunar and Planetary Sciences XXVIII,* Paper presented to the Twenty-Eighth Lunar and Planetary Science Conference (Lunar and Planetary Institute, Houston, Texas, 1997), p. 1489.

47. H. P. Gauggel, C. Geng, H. Schweizer, F. Barth, J. Hommel, R. Winterhoff, and F. Scholz, Electron. Lett. **31,** 367 (1995).
48. B. Pezeshki, J. S. Osinski, H. Zhao, A. Mathur, and T. L. Koch, Electron. Lett. **32,** 2241 (1996).
49. P. Dhamelincourt and J. Barbillat, "Raman Microscopy", in *Handbook of Microscopy–Methods I,* S. Amelinckx, D. vanDyck, J. van Landuyt, and G. van Tendeloo, Eds. (VCH Company, Weinheim/New York/Basel/Cambridge/Tokyo, 1997), Chap. 5, p. 54.